Multiple scattering from gyrotropic bianisotropic cylinders of arbitrary cross sections using the modeling technique

Wen-Yan Yin and Le-Wei Li*
Department of Electrical Engineering, National University of Singapore, 10 Kent Ridge Crescent, Singapore 119260
(Received 10 November 1998)

Based on the principle of the equivolumetric model, the multiple scattering from two-dimensional composite gyrotropic bianisotropic cylinders (GBC's) possessing a certain magnetic group of symmetry is studied by using the indirect modeling technique. At first, a mathematical formulation for the problem is carried out and its solution expressed in terms of a system of simultaneous linear equations of infinite order. The normal incident wave can be either TE_z or TM_z polarization. The linear equation system is then numerically solved by truncating the infinite series. Its numerical results are obtained and presented to characterize the co- and cross-polarized scattering by some typical composite GBC's. Especially, the multiple interactions among all the modeling cylinders, i.e., the host and guest cylinders as well as the guest and guest cylinders, are examined. Some phenomena of the interactions are found and discussed. [S1063-651X(99)05906-1]

PACS number(s): 41.20.−q, 13.40.−f, 03.70.+k, 77.84.Lf

I. INTRODUCTION

In the past few years, the electromagnetic scattering of plane waves by circular bianisotropic cylindrical objects with different constitutive relations and of various geometries has been extensively studied by several researchers [1–7]. These studies were motivated both by interest in developing new techniques for solving scattering problems and by some particular engineering applications. The approaches used for dealing with bianisotropic models are usually the analytical separation variable technique for circular cross sections and numerical techniques (such as the moment and finite-difference methods) for square, rectangular, and other irregular cross sections.

In this paper, we will pay much attention to the multiple interactions in electromagnetic scattering by two-dimensional gyrotropic bianisotropic cylinders (GBC's) of an arbitrary cross section. The approach employed together with the principle of the equivolumetric model in the current analysis is the modeling technique. This technique was first developed by Elsherbeni and Kishk for the modeling of homogeneous isotropic cylindrical objects by circular dielectric and conducting cylinders in 1992 [8]. Recently, it has also been used by Ohki, Shimizu, and Kozaki for modeling the beam-wave scattering from perfectly conducting square cylinders [9]. It is shown in this paper that when a suitable modeling arrangement including the number, location, and size of modeling cylinders is adopted, acceptable results for predicating the scattering features of various bianisotropic cylindrical objects of complex irregular cross sections can be found numerically.

II. GEOMETRY OF THE PROBLEM

According to the modeling pattern adopted in [9], Fig. 1(a) shows the arrangement of 21 GBC's for modeling a two-dimensional inhomogeneous gyrotropic bianisotropic square cylinder with cross section of $0.5\lambda \times 0.5\lambda$, where λ is the incident wavelength. In Fig. 1(a), the host GBC is assumed to be eccentric with the radii $R_h^{(1,l)}$ with respect to the coordinate system $O_h^{(1,l)}(\rho_h^{(1,l)}, \varphi_h^{(1,l)}, z_h^{(1,l)})$ $(l=1,\ldots,M)$; the eccentric distances from $O_h^{(1,2)}, \ldots, O_h^{(1,M)}$ to $O_h^{(1,1)}$ are denoted by $d_{l1}^{(1)}$ $(l=2,\ldots,M)$, correspondingly, and the angle between the line $O_h^{(1,l)}O_h^{(1,1)}$ and the x axis is $\varphi_{l1}^{(1)}$. The radii of 20 guest GBC's are noted by $R_g^{(s)}$ $(s=2,\ldots,21)$ in the local coordinate system $O_g^{(s)}(\rho_g^{(s)}, \varphi_g^{(s)}, z_g^{(s)})$. It should be pointed out that these guest cylinders can be partially or all perfectly conducting, impedance, anisotropic, or isotropic.

Physically, the constitutive characteristics of GBC's here can be described by the following relations in an appropriate frequency range $(e^{i\omega t})$: (i) for the host GBC,

$$\begin{bmatrix} \mathbf{D}_h^{(1,l)}(\omega) \\ \mathbf{B}_h^{(1,l)}(\omega) \end{bmatrix} = \begin{bmatrix} [\varepsilon_h^{(1,l)}(\omega)] & [\xi_{eh}^{(1,l)}(\omega)] \\ [\xi_{mh}^{(1,l)}(\omega)] & [\mu_h^{(1,l)}(\omega)] \end{bmatrix} \begin{bmatrix} \mathbf{E}_h^{(1,l)}(\omega) \\ \mathbf{H}_h^{(1,l)}(\omega) \end{bmatrix},$$

$$l=1,\ldots,M, \tag{1}$$

and (ii) for guest GBC's,

$$\begin{bmatrix} \mathbf{D}_g^{(s)}(\omega) \\ \mathbf{B}_g^{(s)}(\omega) \end{bmatrix} = \begin{bmatrix} [\varepsilon_g^{(s)}(\omega)] & [\xi_{eg}^{(s)}(\omega)] \\ [\xi_{mg}^{(s)}(\omega)] & [\mu_g^{(s)}(\omega)] \end{bmatrix} \begin{bmatrix} \mathbf{E}_g^{(s)}(\omega) \\ \mathbf{H}_g^{(s)}(\omega) \end{bmatrix},$$

$$s=2,\ldots,21, \tag{2}$$

where ω is the operating angular frequency,

$$[\varepsilon_h^{(1,l)}(\omega)]([\varepsilon_g^{(s)}(\omega)]), \quad [\mu_h^{(1,l)}(\omega)]([\mu_g^{(s)}(\omega)]),$$

$$[\xi_{eh}^{(1,l)}(\omega)]([\xi_{eg}^{(s)}(\omega)]), \quad [\xi_{mh}^{(1,l)}(\omega)]([\xi_{mg}^{(s)}(\omega)])$$

are the permittivity tensor, permeability tensor, and magnetoelectric cross-coupling tensors, respectively, and they are all in the gyrotropic form corresponding to different magnetic groups of symmetries [10–13], i.e.,

*FAX: (+65) 779 1103. Electronic address: LWLi@nus.edu.sg

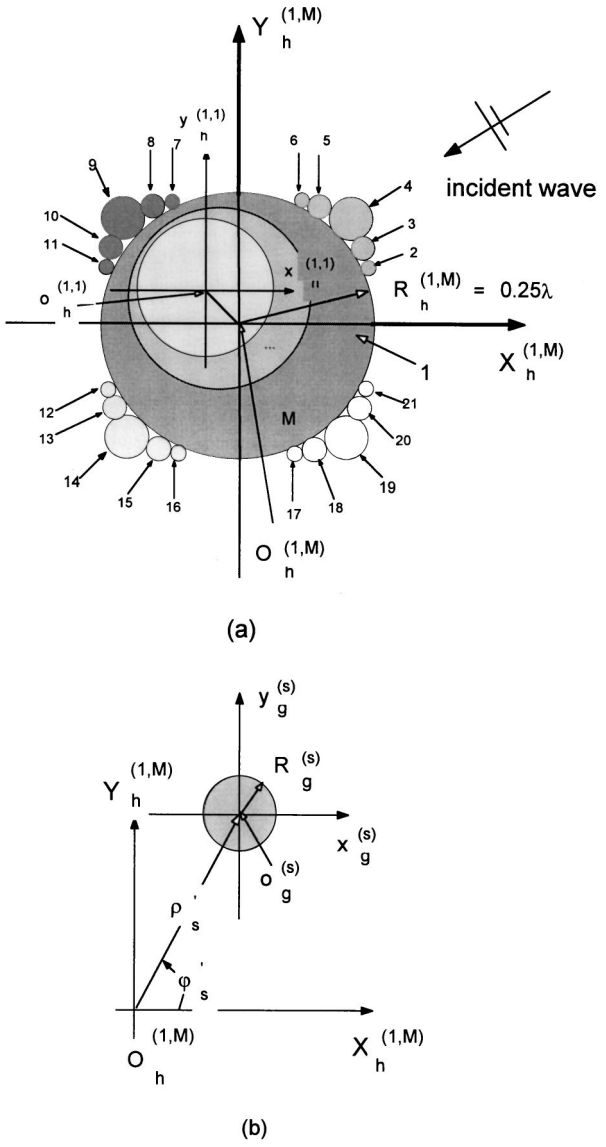

FIG. 1. Geometry and coordinates of 21 parallel circular host and guest GBC's for modeling one GBC with square cross section $0.5\times0.5\lambda^2$. The separation between cylinders q and s ($s\neq q$, $q=1,2,\ldots,21$) is determined by D_{qs}, and usually $R_h^{(1,M)}>R_g^{(s)}$ ($s=2,\ldots,21$). All the cylinders are embedded in an unbounded isotropic medium with permittivity ε_b and permeability μ_b.

$$[C_h^{(1,l)}(\omega)]=\begin{bmatrix} C_{h1}^{(1,l)}(\omega) & iC_{h12}^{(1,l)}(\omega) & 0 \\ -iC_{h12}^{(1,l)}(\omega) & C_{h1}^{(1,l)}(\omega) & 0 \\ 0 & 0 & C_{h2}^{(1,l)}(\omega) \end{bmatrix},$$

$$C=\varepsilon,\mu,\xi_e,\xi_m, \tag{3}$$

$$[C_g^{(s)}(\omega)]=\begin{bmatrix} C_{g1}^{(s)}(\omega) & iC_{g1}^{(s)}(\omega) & 0 \\ -iC_{g1}^{(s)}(\omega) & C_{g1}^{(s)}(\omega) & 0 \\ 0 & 0 & C_{g2}^{(s)}(\omega) \end{bmatrix}. \tag{4}$$

Obviously, both the chiroferrites and chiroplasmas are included here [14–16]. When the magnetoelectric cross-coupling tensors $[\xi_{eh}^{(1,l)}]([\xi_{eg}^{(s)}])$ and $[\xi_{mh}^{(1,l)}]([\xi_{mg}^{(s)}])$ are chosen to be zero, the above GBC's are naturally turned into ordinary ferrite or gyroelectric cylinders. So Eqs. (3) and (4) are of sufficient generality and can incorporate most practical applications.

Using the principle of the equivolumetic model, the guest and host cylinder radii in Fig. 1 should be chosen to be

$$R_h^{(1,M)}=0.2500\lambda, \tag{5a}$$

$$R_g^{(s)}=0.0126\lambda,0.0252\lambda,0.0518\lambda,0.0252\lambda,0.0126\lambda,$$
$$0.0126\lambda,0.0252\lambda,0.0518\lambda,0.0252\lambda,0.0126\lambda,$$
$$s=2,\ldots,21, \tag{5b}$$

and just the same as the volume of the square cylinder per unit,

$$\pi R_h^{(1,M)^2}+\sum_{s=2}^{21}\pi R_g^{(s)^2}=0.25\lambda^2, \tag{5c}$$

while the locations of the 20 guest cylinders with respect to the host cylinder are determined by

$$(\rho_s',\varphi_s')=(0.007878°, 22.3233°),(0.008256°, 30.2203°),$$
$$(0.009053°, 45°),(0.008256°, 59.7796°),$$
$$(0.007878°, 67.6766°),\ldots,(0.009053°, 135°),\ldots,$$
$$(0.009053°, 225°),\ldots,(0.009053°, 315°). \tag{6}$$

Numerically, such arrangements are reasonable and accurate enough for predicting the scattering characteristics of various (in)homogeneous GBC's for a plane-wave (or a beam-wave) incidence of TM_z or TE_z polarization. In fact, changing the number and location of guest cylinders or their constitutive parameters, a large number of different two-dimensional GBC's can be produced, and therefore their scattering features can be understood.

III. FIELD EXPRESSION

The excitation above is provided by a plane electromagnetic (EM) wave, including TM_z and TE_z polarizations simultaneously. With respect to the coordinate system $O_h^{(1,M)}(\rho_h^{(1,M)},\varphi_h^{(1,M)},z_h^{(1,M)})$, the normally incident wave is expressed as

$$\begin{bmatrix} E_z^{\rm inc} \\ H_z^{\rm inc} \end{bmatrix}=\begin{bmatrix} A_{\rm TM}E_0 \\ A_{\rm TE}H_0 \end{bmatrix}e^{ik\rho_h^{(1,M)}\cos(\varphi_h^{(1,M)}-\varphi_0)}, \tag{7}$$

where $k=\omega\sqrt{\mu_b\varepsilon_b}$. For TM_z polarization, $A_{\rm TM}=1$ and $A_{\rm TE}=0$, while for TE_z polarization, $A_{\rm TE}=1$ and $A_{\rm TM}=0$. In the guest coordinate system $O_g^{(s)}(\rho_g^{(s)},\varphi_g^{(s)},z_g^{(s)})$ ($s=2,\ldots,21$), the incident fields are expressed as

$$\begin{bmatrix} E_z^{{\rm inc}(s)} \\ H_z^{{\rm inc}(s)} \\ E_\varphi^{{\rm inc}(s)} \\ H_\varphi^{{\rm inc}(s)} \end{bmatrix}=\sum_{n=-\infty}^{\infty} i^n e^{in(\varphi_g^{(s)}-\varphi_0)}e^{ik\rho_s'\cos(\varphi_s'-\varphi_0)}[\tilde{J}_n^{(s)}]\begin{bmatrix} A_{\rm TM} \\ A_{\rm TE} \end{bmatrix}, \tag{8a}$$

where

$$[\tilde{J}_n^{(s)}]=\begin{bmatrix} J_n^{(s)} & 0 \\ 0 & J_n^{(s)} \\ 0 & i\eta J_n^{(s)\prime} \\ -iJ_n^{(s)\prime}/\eta & 0 \end{bmatrix}, \tag{8b}$$

and $\eta=\sqrt{\mu_b/\varepsilon_b}$, $J_n^{(s)}=J_n(k\rho_g^{(s)})$, $J_n^{(s)\prime}=\partial J_n(x)/\partial x|_{x=k\rho_g^{(s)}}$, whereas $J_n(\cdot)$ is the nth-order Bessel function of the first kind. The scattered fields of the tangential components from the guest cylinders are expressed as

$$\begin{bmatrix} E_z^{\mathrm{sca}(s)} \\ H_z^{\mathrm{sca}(s)} \\ E_\varphi^{\mathrm{sca}(s)} \\ H_\varphi^{\mathrm{sca}(s)} \end{bmatrix}=\sum_{n=-\infty}^{\infty} e^{in\varphi_g^{(s)}}[\tilde{H}_n^{(s)}]\begin{bmatrix} a_n^{(s)} \\ b_n^{(s)} \end{bmatrix}, \tag{9}$$

where $[\tilde{H}_n^{(s)}]=[\tilde{J}_n^{(s)}]_{J\to H}$, and $H_n^{(s)}=H_n^{(1)}(k\rho_g^{(s)})$, $H_n^{(s)\prime}=\partial H_n^{(1)}(x)/\partial x|_{x=k\rho_g^{(s)}}$, $H_n^{(1)}(\cdot)$ is the nth Hankel function of the first kind, and $a(b)_n^{(s)}$ are the unknown scattering coefficients to be determined from the boundary conditions. The scattered field from the host cylinder takes a similar form as Eq. (9) where the unknown scattered coefficients are denoted by $a(b)_n^{(h)}$.

Substituting Eqs. (1) and (2) into Maxwell's equations and using the technique of the generalized separation variables, it is found that the tangential field components in the GBC regions ($\rho_g^{(s)}\leqslant R_g^{(s)}$) in the coordinate system $O_g^{(s)}(\rho_g^{(s)},\varphi_g^{(s)},z_g^{(s)})$ for guest cylinders are written as

$$E_z^{(s)}=\sum_{\pm} E_{z\pm}^{(s)}, \quad H_z^{(s)}=\sum_{\pm} H_{z\pm}^{(s)},$$

$$E_\varphi^{(s)}=\sum_{\pm} E_{\varphi\pm}^{(s)}, \quad H_\varphi^{(s)}=\sum_{\pm} H_{\varphi\pm}^{(s)}, \tag{10a}$$

and

$$\begin{bmatrix} E_{z\pm}^{(s)} \\ H_{z\pm}^{(s)} \\ E_{\varphi\pm}^{(s)} \\ H_{\varphi\pm}^{(s)} \end{bmatrix}=\sum_{n=-\infty}^{\infty}\begin{bmatrix} X_{1\pm}^{(s)} \\ X_{3\pm}^{(s)} \\ X_{5\pm}^{(s)} \\ X_{7\pm}^{(s)} \end{bmatrix} D_{1n\pm}^{(s)} e^{in\varphi_g^{(s)}}, \tag{10b}$$

where $X_{\nu\pm}^{(s)}$ ($\nu=1,3,5,7$) can be obtained by following the ways adopted in [2,3] and their expressions are suppressed here: $D_{1n\pm}^{(s)}$ are the unknown mode expanding coefficients. For the host cylinder, the tangential field components in the lth layer ($l=1,\ldots,M$) are expressed similarly to that in Eq. (10a), i.e.,

$$E_z^{(1,l)}=\sum_{\pm} E_{z\pm}^{(1,l)}, \quad H_z^{(1,l)}=\sum_{\pm} H_{z\pm}^{(1,l)},$$

$$E_\varphi^{(1,l)}=\sum_{\pm} E_{\varphi\pm}^{(1,l)}, \quad H_\varphi^{(1,l)}=\sum_{\pm} H_{\varphi\pm}^{(1,l)}, \tag{11a}$$

and in the coordinate system $O_h^{(1,1)}(\rho_h^{(1,1)},\varphi_h^{(1,1)},z_h^{(1,1)})$,

$$\begin{bmatrix} E_{z\pm}^{(1,l)} \\ H_{z\pm}^{(1,l)} \\ E_{\varphi\pm}^{(1,l)} \\ H_{\varphi\pm}^{(1,l)} \end{bmatrix}=\sum_{n=-\infty}^{\infty}\begin{bmatrix} X_{1\pm}^{(1,l)} & X_{2\pm}^{(1,l)} \\ X_{3\pm}^{(1,l)} & X_{4\pm}^{(1,l)} \\ X_{5\pm}^{(1,l)} & X_{6\pm}^{(1,l)} \\ X_{7\pm}^{(1,l)} & X_{8\pm}^{(1,l)} \end{bmatrix}\begin{bmatrix} D_{1n\pm}^{(1,l)} \\ (1-\delta_{l1})D_{2n\pm}^{(1,l)} \end{bmatrix} e^{in\varphi_h^{(1,1)}}, \tag{11b}$$

where $X_{\nu\pm}^{(1,l)}$ ($\nu=1,\ldots,8$) are presented in Appendix A,

$$\delta_{l1}=\begin{cases} 1, & l=1, \\ 0, & l=2,\ldots,M, \end{cases}$$

and $D_{1n\pm}^{(1,l)}$ and $D_{2n\pm}^{(1,l)}$ are also the unknown mode expanding coefficients.

To determine the unknown mode expanding coefficients, the boundary conditions for the tangential components of the electric and magnetic fields at $\rho_h^{(1,l)}=R_h^{(1,l)}$ ($2\leqslant l<M$) are to be enforced. This requires that the fields (11b) must be translated into the coordinate system $O_h^{(1,l)}(\rho_h^{(1,l)},\varphi_h^{(1,l)},z_h^{(1,l)})$ using the translational addition theorem (TATM) for cylindrical wave functions, i.e.,

$$\begin{aligned} &Z_n(\sqrt{S_\pm^{(1,l)}}\rho_h^{(1,1)})e^{in\varphi_h^{(1,1)}} \\ &\quad=\sum_{m=-\infty}^{+\infty} Z_{m-n}(\sqrt{S_\pm^{(1,l)}}d_{l1}^{(1)})Z_m(\sqrt{S_\pm^{(1,l)}}\rho_h^{(1,l)}) \\ &\qquad\times e^{i[m\varphi_h^{(1,l)}-(m-n)\varphi_{l1}^{(1)}]}. \end{aligned} \tag{12}$$

So Eq. (11b) becomes

$$\begin{bmatrix} E_{z\pm}^{(1,l)} \\ H_{z\pm}^{(1,l)} \\ E_{\varphi\pm}^{(1,l)} \\ H_{\varphi\pm}^{(1,l)} \end{bmatrix}=\sum_{m=-\infty}^{+\infty}\sum_{n=-\infty}^{+\infty}\begin{bmatrix} \tilde{X}_{1\pm}^{(1,l)} & \tilde{X}_{2\pm}^{(1,l)} \\ \tilde{X}_{3\pm}^{(1,l)} & \tilde{X}_{4\pm}^{(1,l)} \\ \tilde{X}_{5\pm}^{(1,l)} & \tilde{X}_{6\pm}^{(1,l)} \\ \tilde{X}_{7\pm}^{(1,l)} & \tilde{X}_{8\pm}^{(1,l)} \end{bmatrix}\times\begin{bmatrix} D_{1n\pm}^{(1,l)} \\ (1-\delta_{l1})D_{2n\pm}^{(1,l)} \end{bmatrix} e^{im\varphi_h^{(1,l)}}, \tag{13}$$

where $\tilde{X}_{\nu\pm}^{(1,l)}$ ($\nu=1,\ldots,8$) are also presented in Appendix A.

To enforce the boundary conditions on the external surface $\rho_h^{(1,M)}=R_h^{(1,M)}$ and $\rho_g^{(s)}=R_g^{(s)}$ ($s=2,\ldots,21$), the TATM shown in Appendix B for the Hankel function should be employed. Furthermore, 21 system equations of infinite order for 21 cylinders can be derived, and for the host cylinder,

$$\begin{aligned} &[X_{MM}^{(1)}]_{L\times L}[X^{(1)}]_{L\times L}^{-1}[X_{11}^{(1,1)}]_{L\times L}[D_{1\pm}^{(1)}]_{L\times 1} \\ &\quad-[\tilde{H}_{mM}^{(1)}]\begin{bmatrix} a_m^{(h)} \\ b_m^{(h)} \end{bmatrix}-[\tilde{J}_{mM}^{(1)}]\sum_{s=2}^{21}\sum_{n=-\infty}^{+\infty} H_{m-n}^{(1)}(k\rho_s') \\ &\quad\times e^{-i(m-n)\varphi_s'}\begin{bmatrix} \alpha_n^{(s)} \\ b_n^{(s)} \end{bmatrix} \\ &\quad=i^m e^{-im\varphi_0}e^{ik\rho_h^{(1,M)}}[\tilde{J}_{mM}^{(1)}]\begin{bmatrix} A_{\mathrm{TM}} \\ A_{\mathrm{TE}} \end{bmatrix}, \end{aligned} \tag{14}$$

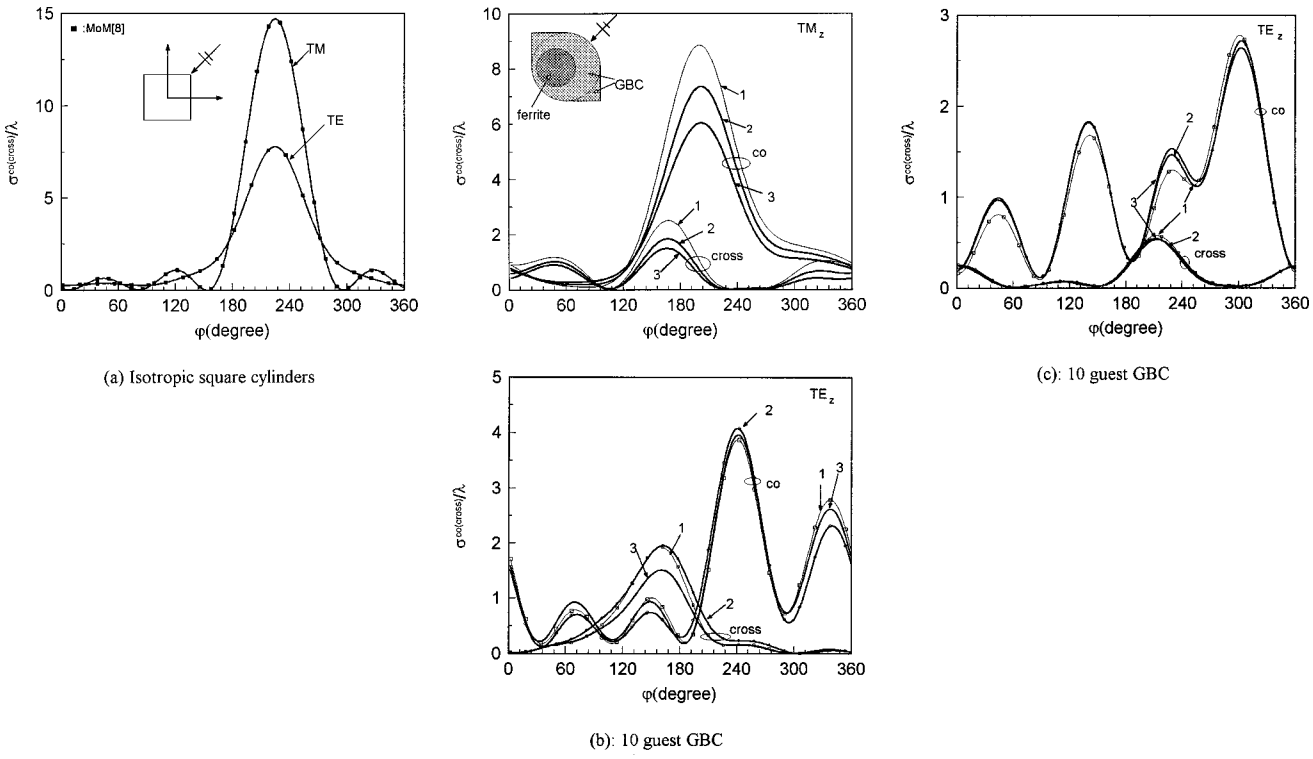

FIG. 2. $\sigma^{\mathrm{co(cross)}}$ versus φ for an isotropic square cylinder ($0.5\lambda \times 0.5\lambda$) and two eccentric GBC cylinders.

where $[X^{(1)}]_{L\times L}$ are shown in Appendix C and the third term on the left side of Eq. (14) accounts for the multiple interactions between the host and guest cylinders. For all the guest cylinders, a similar equation system can be obtained, i.e.,

$$[X^{(s)}][D_{\pm}^{(s)}]_{L\times 1}-[\tilde{H}_m^{(s)}]\begin{bmatrix} a_m^{(s)} \\ b_m^{(s)} \end{bmatrix} -[\tilde{J}_m^{(s)}]\sum_{\substack{q=2\\ q\neq s}}^{21}\sum_{n=-\infty}^{+\infty} H_{m-n}^{(1)}(kD_{qs}) \times e^{-i(m-n)\varphi'_{qs}}\begin{bmatrix} a_n^{(q)} \\ b_n^{(q)} \end{bmatrix} = i^m e^{-im\varphi_0} e^{ik\rho'_s\cos(\varphi'_s-\varphi_0)}[\tilde{J}_m^{(s)}]\begin{bmatrix} A_{\mathrm{TM}} \\ A_{\mathrm{TE}} \end{bmatrix}, \quad (15)$$

where $[D_{\pm}^{(s)}]_{L\times 1}=[D_{1n+}^{(s)}\ D_{1n-}^{(s)}\ 0\ 0]^T$ and the third term on the left side of Eq. (15) also accounts for the multiple-scattering contributions among all the modeling cylinders.

To find a solution of the unknown coefficients $a(b)_n^{(h)}$ and $a(b)_n^{(s)}$ $(s=2,\ldots,21)$, all equation systems must be properly truncated to form a finite matrix system and then solved numerically after such a truncation. Physical intuition suggests that the truncation number $N_0\{m,n=-N_0,\ldots,N_0, L=4(2N_0+1)\}$ depends mainly on the electric size of $\max\{kR_h^{(1,M)}\}$. Since $R_h^{(1,M)}>R_g^{(s)}$, N_0 becomes not very large for the electrically nonlarge case, so that a numerical solution is feasible. The far-zone scattered field can be computed after using the large argument approximation of the Hankel function, and the corresponding formulations for determining of the co- and cross-polarized echo widths $\sigma^{\mathrm{co(cross)}}$ can be found in [5].

IV. NUMERICAL RESULTS AND DISCUSSION

Some computer FORTRAN codes have been developed in this paper for calculating the co- and cross-polarized echo widths $\sigma^{\mathrm{co(cross)}}$ of various GBC's. For practical considerations, we first let $\varepsilon_b=\varepsilon_0$ and $\mu_b=\mu_0$. At first, the validity of our codes, including the accuracy and convergence rate, have been checked indirectly by computing the normalized $\sigma^{\mathrm{co}}/\lambda$ of isotropic square cylinder as shown as in Fig. 2(a). It is clear that excellent agreement has been achieved between the results in this paper and that obtained by the method of moments [8]. The parameters used for calculations are chosen to be $f=10\,\mathrm{GHz}$, $N_0\geqslant 8$, and $\varphi_0=45°$, for the following.

Case (a): $[\varepsilon_h^{(1,1)}]=[\varepsilon_g^{(s)}]=4.0\varepsilon_0\bar{\bar{I}}$, $[\mu_h^{(1,1)}]=[\mu_g^{(s)}]=\mu_0\bar{\bar{I}}$,

$$[\xi_{eh}^{(1,1)}]=-[\xi_{mh}^{(1,1)}]=-i10^{-6}\sqrt{\mu_0\varepsilon_0}\bar{\bar{I}},$$

$$[\xi_{eg}^{(s)}]=-[\xi_{mg}^{(s)}]=-i10^{-5}\sqrt{\mu_0\varepsilon_0}\bar{\bar{I}}, \quad s=2,\ldots,21.$$

Case (b): $k_0R_h^{(1,1)}=0.942$, $\varphi_{21}^{(1)}=0°$, $k_0d_{21}^{(1)}=0.419$,

$$[\varepsilon_h^{(1,1)}]=12.6\varepsilon_0\bar{\bar{I}}, \quad \mu_{h2}^{(1,l)}=\mu_0,$$

$$\mu_{h1}^{(1,l)}=\mu_0\omega_{h0}^{(1,l)}\omega_{hm}^{(1,l)}/[\omega_{h0}^{(1,l)^2}-\omega^2],$$

$$\mu_{h12}^{(1,l)}=-\mu_0\omega\omega_{hm}^{(1,l)}/[\omega_{h0}^{(1,l)^2}-\omega^2],$$

$$M_{hs}^{(1,l)}\mu_0=0.275T, \quad \omega_{hm}^{(1,l)}=2.21\times 10^5 M_{hs}^{(1,l)},$$

$$l=1,2, \quad \omega_{h0}^{(1,1)}/\omega_{hm}^{(1,1)}=0.6,$$

$$\omega_{h0}^{(1,2)}/\omega_{hm}^{(1,2)}=0.1,\quad [\xi_{eh}^{(1,1)}]=-[\xi_{mh}^{(1,1)}]=-i10^{-6}\sqrt{\mu_0\varepsilon_0}\bar{\bar{I}},$$

$$[\varepsilon_h^{(1,2)}]=[\varepsilon_g^{(s)}]=\varepsilon_0\begin{bmatrix}4.0 & i0.5 & 0\\ -i0.5 & 4.0 & 0\\ 0 & 0 & 4.5\end{bmatrix},$$

$$[\mu_h^{(1,2)}]=[\mu_g^{(s)}],\quad s=2,\ldots,11,$$

$$[\xi_{eh}^{(1,2)}]=-[\xi_{mh}^{(1,2)}]=[\xi_{eg}^{(s)}]=-[\xi_{mg}^{(s)}]$$
$$=\sqrt{\mu_0\varepsilon_0}\begin{bmatrix}-i0.6 & -0.3 & 0\\ 0.3 & -i0.6 & 0\\ 0 & 0 & -i0.8\end{bmatrix}(D_\infty);$$

Case (c): the parameters are the same as (b), except that

$$[\xi_{eh}^{(1,2)}]=[\xi_{mh}^{(1,2)}]=[\xi_{eg}^{(s)}]=[\xi_{mg}^{(s)}]$$
$$=\sqrt{\mu_0\varepsilon_0}\begin{bmatrix}-i0.6 & -0.3 & 0\\ 0.3 & -i0.6 & 0\\ 0 & 0 & -i0.8\end{bmatrix}(C_{\infty\nu}).$$

In Fig. 2(a), we let $[\xi_{eh}^{(1,1)}]=-[\xi_{mh}^{(1,1)}]=-i10^{-6}\sqrt{\mu_0\varepsilon_0}\bar{\bar{I}}$ and $[\xi_{eg}^{(s)}]=-[\xi_{mg}^{(s)}]=-i10^{-5}\sqrt{\mu_0\varepsilon_0}\bar{\bar{I}}$ $(s=2,\ldots,21)$; so they have no contribution to the copolarized echo width for TM_z or TE_z incidence. Comparing Fig. 2(a) with the results shown in [8], it is clear that our modeling arrangement is much more accurate. In Figs. 2(b) and 2(c), the core of the eccentric GBC is assumed to be ordinary ferrite with internal bias field intensity $\omega_{h0}^{(1,1)}/\omega_{hm}^{(1,1)}=0.6$, and the modeling arrangement is produced by removing guest GBC's {1,2,3,4,5} and {12,13,14,15,16} from Fig. 1(a). Therefore, the locations of the remaining ten guest GBC's are determined by $(\rho_s',\varphi_s')=7(0.007878,112.3233°)$, 8(0.008256, 120.2203°), 9(0.009053,135°), 10(0.008256,149.7796°), 11(0.007878,157.6766°), 17(0.007878,292.3233°), 18(0.008256,300.2203°), 19(0.009053,315°), 20(0.008256, 329.7796°), and 21(0.007878,337.6766°), respectively. The constitutive tensors of the guest GBC's are chosen to be the same as the outer layer's constitutive tensor of the host cylinder $(M=2)$. They correspond to continuous magnetic groups of symmetries D_∞ and $C_{\infty\nu}$ [10]. Especially, in Figs. 2(b) and 2(c) the multiple interactions between the guest and host GBC, Eq. (1), as well as the guest GBC's, are demonstrated for $\sigma^{\mathrm{co(cross)}}$. Here curve 1 represents that only the multiple scattering between 1⇔7, 1⇔8, 1⇔9, 1⇔10, 1⇔11, 1⇔17, 1⇔18, 1⇔19, 1⇔20, and 1⇔21 is considered, while the multiple scattering among all the guest GBC's {7,8,9,10,11,17,18,19,20, 21} is not included. For curve 2, only the interactions of 21⇔1⇔7, 7⇔1⇔8, 8⇔1⇔9, 9⇔1⇔10, 10⇔1⇔11, 11⇔1⇔17, 17⇔1⇔18, 18⇔1⇔19, 19⇔1⇔20, and 20⇔1⇔21 are taken into account. Curve 3 stands for the most general case in which all possible multiple-scattering contributions are considered. With respect to the locations of two groups of guest GBC's {7,8,9,10,11} and {17,18,19,20,21}, the incident wave in the $\varphi_0=45°$ direction is just the broadside incidence. Physically, Fig. 2(b) suggests that, for TM_z incidence the effect of multiple interactions between two groups of guest GBC's is a little bit stronger for σ^{co} than that of the TE_z case. In addition, it is very interesting to note that, for the TE_z case, good agreement is achieved among the curves 1, 2, and 3 in Fig. 2(c) for σ^{cross}.

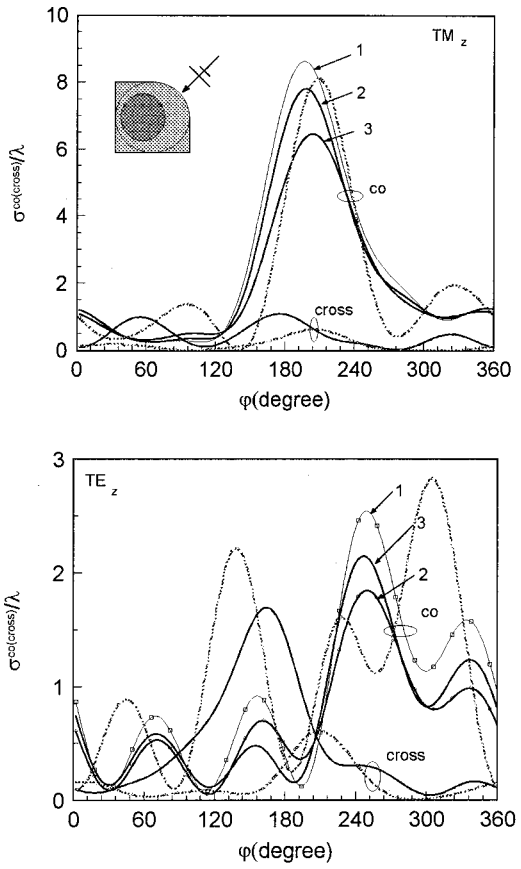

FIG. 3. $\sigma^{\mathrm{co(cross)}}$ versus φ for an eccentric GBC cylinder $f=10$ GHz, $N_0=8$, and $\varphi_0=45°$.

Furthermore, Fig. 3 depicts the cross section $\sigma^{\mathrm{co(cross)}}$ of a composite GBC corresponding to two kinds of constitutive models for TM_z- and TE_z-wave incidences, respectively. The solid line in Fig. 3 stands for the parameters used for the calculation being the same as in Fig. 2(b) except that 15 guest GBC's are used. For the dotted line the parameters are the same as in Fig. 2(c) (15 guest GBC's).

In Fig. 3, the locations of the 15 guest GBC's are given by $(\rho_s',\varphi_s')_{s=15}=(\rho_s',\varphi_s')_{s=10}+\{12(0.007878,202.3233°)$, 13(0.008256,210.2203°), 14(0.009053,225°), 15(0.008256, 239.7796°), 16(0.007878,247.6766°)}, and the dotted lines represent the case of continuous magnetic group of symmetry $C_{\infty\nu}$ [10]. For curve 1, only the multiple scattering between 1⇔7, 1⇔8, 1⇔9, 1⇔10, 1⇔11, 1⇔12, 1⇔13, 1⇔14, 1⇔15, 1⇔16, 1⇔17, 1⇔18, 1⇔19, 1⇔20, and 1⇔21 is considered. Similarly, for curve 2, only the interactions of 21⇔1⇔7, 7⇔1⇔8, 8⇔1⇔9, 9⇔1⇔10, 10⇔1⇔11, 11⇔1⇔12, 12⇔1⇔13, 13⇔1⇔14, 14⇔1⇔15, 15⇔1⇔16, 16⇔1⇔17, 17⇔1⇔18, 18⇔1⇔19, 19⇔1⇔20, and 20⇔1⇔21 are included. By comparing the curves of the TE_z-wave incidence with those in Fig. 2(b), it can be seen that (i) the multiple interactions among the modeling cylinders are enhanced due to the introduction of cylinders {12,13,14,15,16} in the forward range of the incident wave and (ii) for both incidences all multiple-scattering contributions must be considered. On the other hand, it is obvious

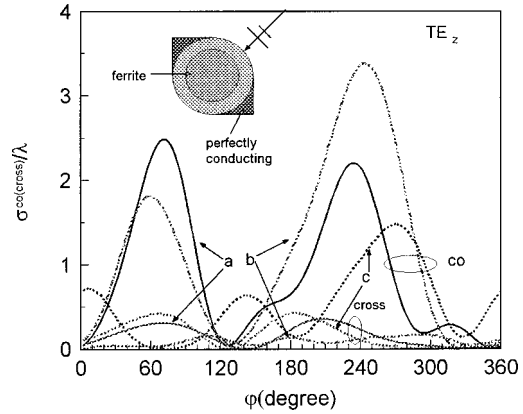

FIG. 4. $\sigma^{\mathrm{co(cross)}}$ versus φ for a concentric composite cylinder.

that in Fig. 3, compared to the magnetic group of symmetry D_∞, stronger co- and weaker cross-polarized scattered field components for the symmetry $C_{\infty v}$ can be expected for either TM_z- or TE_z-wave incidence.

Figure 4 shows the $\sigma^{\mathrm{co(cross)}}$ of a composite concentric perfectly conducting and GBC for a TE_z-wave case, in which the darkened regions are assumed to be perfectly conducting. The parameters are chosen to be $f=10\,\mathrm{GHz}$,

$$N_0 \geqslant 8, \quad \varphi_0 = 45°, \quad k_0 d_{21}^{(1)} = 0.0,$$

$$[\varepsilon_h^{(1,1)}] = 12.6\varepsilon_0 \bar{\bar{I}}, \quad \mu_{h2}^{(1,l)} = \mu_0,$$

$$\mu_{h1}^{(1,l)} = \mu_0 \omega_{h0}^{(1,l)} \omega_{hm}^{(1,l)} / [\omega_{h0}^{(1,l)2} - \omega^2],$$

$$\mu_{h12}^{(1,l)} = -\mu_0 \omega \omega_{hm}^{(1,l)} / [\omega_{h0}^{(1,l)2} - \omega^2],$$

$$M_{hs}^{(1,l)} \mu_0 = 0.275T, \quad \omega_{hm}^{(1,l)} = 2.21 \times 10^5 M_{hs}^{(1,l)},$$

$$l = 1,2, \quad \omega_{h0}^{(1,1)} / \omega_{hm}^{(1,1)} = 0.6,$$

$$[\xi_{eh}^{(1,1)}] = -[\xi_{mh}^{(1,1)}] = -i10^{-6}\sqrt{\mu_0 \varepsilon_0}\bar{\bar{I}},$$

$$[\xi_{eh}^{(1,2)}] = -[\xi_{mh}^{(1,2)}] = \sqrt{\mu_0 \varepsilon_0} \begin{bmatrix} -i0.6 & -0.3 & 0 \\ 0.3 & -i0.6 & 0 \\ 0 & 0 & -i0.8 \end{bmatrix},$$

$$[\varepsilon_h^{(1,2)}] = \varepsilon_0 \begin{bmatrix} 4.0 & i0.5 & 0 \\ -i0.5 & 4.0 & 0 \\ 0 & 0 & 4.5 \end{bmatrix} (D^\infty),$$

$\omega_{h0}^{(1,2)} / \omega_{hm}^{(1,2)} = 0.1$ (a), 1.0 (b), and 2.5 (c).

In Fig. 4, the location and geometrical size of the ten perfectly conducting guest cylinders are the same as in Fig. 2(b), while the internal bias field intensity $\omega_{h0}^{(1,2)} / \omega_{hm}^{(1,2)}$ of the host GBC is increased from 0.1 to 1.0 to 2.5. Under such circumstances, $\sigma^{\mathrm{co(cross)}}$ can still be adjusted effectively as in ordinary ferrite by varying the biasing field intensity or its direction. On the other hand, numerical experiments can prove that the multiple interactions among the modeling cylinders are enhanced greatly since the guest cylinders are the perfectly conducting strong scatters.

Finally, Fig. 5 depicts the $\sigma^{\mathrm{co(cross)}}$ of a composite eccentric perfectly conducting and GBC square cylinder for a

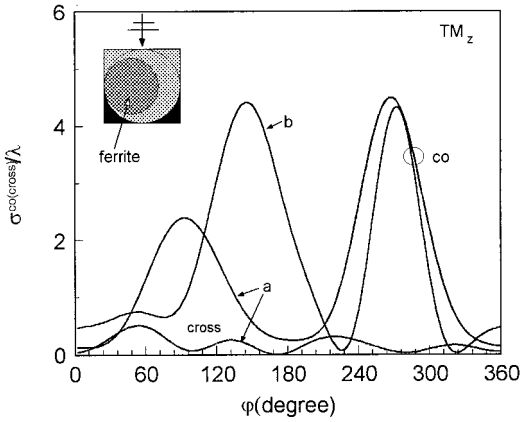

FIG. 5. $\sigma^{\mathrm{co(cross)}}$ versus φ for a composite concentric perfectly conducting and GBC square cylinder ($0.5\lambda \times 0.5\lambda$).

TM_z-wave incidence, and the ordinary gyroelectric case is also shown ($f=10$ GHz, $\varphi_0=90°$, $k_0 d_{21}^{(1)}=0.628$, $N_0=8$). For case (a) the parameters of the ferrite and GBC regions are the same as in Fig. 2(b), while for case (b) the parameters are the same as (b), except that

$$[\xi_{eh}^{(1,2)}] = -[\xi_{mh}^{(1,2)}] = [\xi_{eg}^{(s)}] = -[\xi_{mg}^{(s)}] = -i10^{-5}\sqrt{\mu_0 \varepsilon_0}\bar{\bar{I}},$$

$s=2, \ldots, 11$ (ordinary gyroelectric medium).

In Fig. 5, the darkened regions are perfectly conducting, and the location and geometrical size of the ten PCC's and ten GBC's (ten GEC's) are the same as in Fig. 1. In the modeling of such a composite structure, all multiple interactions between different PCC's and GBC's are also taken into account, and for case (b), no cross-polarized scattered field component can be expected for this ordinary composite gyroelectric square cylinder for either normal TM_z- or TE_z-wave incidence.

V. CONCLUSION

The electromagnetic scattering from some two-dimensional composite gyrotropic bianisotropic cylinders has been investigated, and our attention has been paid to the multiple interactions among the modeling cylinders. Also, the global effects of the geometrical and constitutive parameters of gyrotropic bianisotropic cylindrical structures corresponding to different magnetic groups of symmetries on the co- and cross-polarized echo widths have been examined carefully. It has been proved that the indirect modeling technique possesses the advantages of simplicity and efficiency under some circumstances.

ACKNOWLEDGMENT

This work has been supported by the Research Project No. RP3981676 from the National University of Singapore.

APPENDIX A

In Eq. (11b), the related variables with respect to the coordinate system $O_h^{(1,1)}(\rho_h^{(1,1)}, \varphi_h^{(1,1)}, z_h^{(1,1)})$ are expressed by

$$X_{1\pm}^{(1,l)}=S_{\pm}^{(1,l)}J_{nl\pm}^{(1,1)},$$

$$X_{2\pm}^{(1,l)}=S_{\pm}^{(1,l)}N_{nl\pm}^{(1,1)},$$

$$X_{3\pm}^{(1,l)}=q_{\pm}^{(1,l)}J_{nl\pm}^{(1,1)},$$

$$X_{4\pm}^{(1,l)}=q_{\pm}^{(1,l)}N_{nl\pm}^{(1,1)},$$

$$X_{5\pm}^{(1,l)}=-M_{\pm}^{(1,l)}J_{nl\pm}^{(1,1)\prime}-\frac{inN_{\pm}^{(1,l)}}{\rho_h^{(1,1)}}J_{nl\pm}^{(1,1)},$$

$$X_{6\pm}^{(1,l)}=-M_{\pm}^{(1,l)}N_{nl\pm}^{(1,1)\prime}-\frac{inN_{\pm}^{(1,l)}}{\rho_h^{(1,1)}}N_{nl\pm}^{(1,1)},$$

$$X_{7\pm}^{(1,l)}=-X_{\pm}^{(1,l)}J_{nl\pm}^{(1,1)\prime}-\frac{inY_{\pm}^{(1,l)}}{\rho_h^{(1,1)}}J_{nl\pm}^{(1,1)},$$

$$X_{8\pm}^{(1,l)}=-X_{\pm}^{(1,l)}N_{nl\pm}^{(1,1)\prime}-\frac{inY_{\pm}^{(1,l)}}{\rho_h^{(1)}}N_{nl\pm}^{(1,1)} \tag{A1}$$

and

$$J_{nl\pm}^{(1,j)}=J_n(\sqrt{S_{\pm}^{(1,l)}}\rho_h^{(1,j)}),$$

$$N_{nl\pm}^{(1,j)}=N_n(\sqrt{S_{\pm}^{(1,j)}}\rho_h^{(i,j)}),$$

$$J_{nl\pm}^{(1,j)\prime}=J_n'(\sqrt{S_{\pm}^{(1,l)}}\rho_h^{(1,j)}),$$

$$N_{nl\pm}^{(1,l)\prime}=N_n'(\sqrt{S_{\pm}^{(1,l)}}\rho_h^{(1,j)}),$$

$$l=1,2,\ldots,M, \tag{A2}$$

and

$$M_{\pm}^{(1,l)}=\sqrt{S_{\pm}^{(1,l)}}(A_{21}^{(1,l)}S_{\pm}^{(1,l)}+A_{41}^{(1,l)}Q_{\pm}^{(1,l)}),$$

$$N_{\pm}^{(1,l)}=A_{22}^{(1,l)}S_{\pm}^{(1,l)}+A_{42}^{(1,l)}Q_{\pm}^{(1,l)},$$

$$X_{\pm}^{(1,l)}=\sqrt{S_{\pm}^{(1,l)}}(A_{23}^{(1,l)}S_{\pm}^{(1,l)}+A_{43}^{(1,l)}Q_{\pm}^{(1,l)}),$$

$$Y_{\pm}^{(1,l)}=A_{24}^{(1,l)}S_{\pm}^{(1,l)}+A_{44}^{(1,l)}Q_{\pm}^{(1,l)},$$

$$S_{\pm}^{(1,l)}=\frac{-(P_1^{(1,l)}+P_4^{(1,l)})\pm\sqrt{(P_1^{(1,l)}-P_4^{(1,l)})^2-4P_2^{(1,l)}P_3^{(1,l)}}}{2},$$

$$Q_{\pm}^{(1,l)}=-i\frac{S_{\pm}^{(1,l)}(S_{\pm}^{(1,l)}+P_1^{(1,l)})}{P_2^{(1,l)}}, \tag{A3}$$

$$P_1^{(1,l)}=i\omega\frac{A_{21}^{(1,l)}\varepsilon_{h2}^{(1,l)}(\omega)+A_{23}^{(1,l)}\xi_{mh2}^{(1,l)}(\omega)}{\Delta_l^{(1)}},$$

$$P_2^{(1,l)}=-\omega\frac{A_{43}^{(1,l)}\mu_{h2}^{l(1,l)}(\omega)+A_{41}^{(1,l)}\xi_{eh2}^{(1,l)}(\omega)}{\Delta_l^{(1)}},$$

$$P_3^{(1,l)}=\omega\frac{A_{21}^{(1,l)}\varepsilon_{h2}^{(1,l)}(\omega)+A_{23}^{(1,l)}\xi_{mh2}^{(1,l)}(\omega)}{\Delta_l^{(1)}},$$

$$P_4^{(1,l)}=-i\omega\frac{A_{21}^{(1,l)}\xi_{eh2}^{(1,l)}(\omega)+A_{23}^{(1,l)}\mu_{h2}^{(1,1)}(\omega)}{\Delta_l^{(1)}},$$

$$\Delta_l^{(1)}=A_{21}^{(1,l)}A_{43}^{(1,l)}-A_{23}^{(1,l)}A_{41}^{(1,l)}, \tag{A4}$$

$$\begin{bmatrix} A_{11}^{(1,l)} & A_{21}^{(1,l)} & A_{31}^{(1,l)} & A_{41}^{(1,l)} \\ A_{12}^{(1,l)} & A_{22}^{(1,l)} & A_{32}^{(1,l)} & A_{42}^{(1,l)} \\ A_{13}^{(1,l)} & A_{23}^{(1,l)} & A_{33}^{(1,l)} & A_{43}^{(1,l)} \\ A_{14}^{(1,l)} & A_{24}^{(1,l)} & A_{34}^{(1,l)} & A_{44}^{(1,l)} \end{bmatrix}=\begin{bmatrix} -\omega\xi_{mh12}^{(1,l)}(\omega) & i\omega\xi_{mh1}^{(1,l)}(\omega) & -\omega\mu_{h12}^{(1,l)}(\omega) & i\omega\mu_{h1}^{(1,l)}(\omega) \\ -i\omega\xi_{mh1}^{(1,l)}(\omega) & -\omega\xi_{mh12}^{(1,l)}(\omega) & -i\omega\mu_{h1}^{(1,l)}(\omega) & -\omega\mu_{h12}^{(1,l)}(\omega) \\ \omega\varepsilon_{h12}^{(1,l)}(\omega) & -i\omega\varepsilon_{h1}^{(1,l)}(\omega) & \omega\xi_{eh12}^{(1,l)}(\omega) & -i\omega\xi_{eh1}^{(1,l)}(\omega) \\ i\omega\varepsilon_{h1}^{(1,l)}(\omega) & \omega\varepsilon_{h12}^{(1,l)}(\omega) & i\omega\xi_{eh1}^{(1,l)}(\omega) & \omega\xi_{eh12}^{(1,l)}(\omega) \end{bmatrix}^{-1}, \tag{A5}$$

while in the coordinate system $O_h^{(1,l)}(\rho_h^{(1,l)},\varphi_h^{(1,l)},z_h^{(1,l)})$,

$$\tilde{X}_{\nu\pm}^{(1,l)}=e^{-i(m-n)\varphi_{l1}^{(1)}}X_{\nu\pm}^{(1,l)}|_{(J,H)\to(\tilde{J},\tilde{H});1\to l}, \tag{A6a}$$

$$\tilde{J}_{mn\pm}^{(1,l)}=J_m(\sqrt{S_{\pm}^{(1,l)}}\rho_h^{(1,l)}J_{m-n}(\sqrt{S_{\pm}^{(1,l)}}d_{l1}^{(1)}),$$

$$\tilde{H}_{mn\pm}^{(1,l)}=H_m^{(1)}(\sqrt{S_{\pm}^{(1,l)}}\rho_h^{(1,l)})J_{m-n}(\sqrt{S_{\pm}^{(1,l)}}d_{l1}^{(1)}). \tag{A6b}$$

APPENDIX B

To transform the scattered fields of the sth guest cylinder ($s=2,\ldots,21$) with respect to $O_g^{(s)}(\rho_g^{(s)},\varphi_g^{(s)},z_g^{(s)})$ to the qth guest coordinate $O_g^{(q)}(\rho_g^{(q)},\varphi_g^{(q)},z_g^{(q)})$ ($s\neq q$), we must have

$$H_n^{(1)}(k\rho_g^{(s)})e^{in\varphi_g^{(s)}}=\sum_{m=-\infty}^{+\infty}H_{m-n}^{(1)}(kD_{qs})J_m(k\rho_g^{(q)})e^{i[m\varphi_g^{(q)}-(m-n)\varphi_{qs}]} \tag{B1a}$$

and

$$D_{qs}^2=\rho_q'^2+\rho_s'^2-2\rho_q'\rho_s'\cos(\varphi_q'-\varphi_s'), \tag{B1b}$$

$$\varphi_{qs}=\begin{cases}\cos^{-1}\left(\dfrac{\rho_q'\cos\varphi_q'-\rho_s'\cos\varphi_s'}{D_{qs}}\right), & \rho_q'\sin\varphi_q'\geqslant\rho_s'\sin\varphi_s',\\ -\cos^{-1}\left(\dfrac{\rho_q'\cos\varphi_q'-\rho_s'\cos\varphi_s'}{D_{qs}}\right), & \rho_q'\sin\varphi_q'<\rho_s'\sin\varphi_s'.\end{cases} \tag{B1c}$$

APPENDIX C

The boundary equations at $\rho_h^{(1,l)}=R_h^{(1,1)},R_h^{(1,2)},\ldots,R_h^{(1,p)},\ldots,R_h^{(1,M-1)}$ can be expressed as

$$[X_{11}^{(1)}]_{L\times L}[D_{1\pm}^{(1)}]_{L\times 1}=[X_{12}^{(1)}]_{L\times L}[D_{2\pm}^{(1)}]_{L\times 1}, \tag{C1a}$$

$$[X_{22}^{(1)}]_{L\times L}[D_{2\pm}^{(1)}]_{L\times 1}=[X_{23}^{(1)}]_{L\times L}[D_{3\pm}^{(1)}]_{L\times 1}, \tag{C1b}$$

$$[X_{pp}^{(1)}]_{L\times L}[D_{p\pm}^{(1)}]_{L\times 1}=[X_{p(p+1)}^{(1)}]_{L\times L}[D_{p+1\pm}^{(1)}]_{L\times 1}, \tag{C1c}$$

$$[X_{(M-1)(M-1)}^{(1)}]_{L\times L}[D_{M-1\pm}^{(1)}]_{L\times 1}=[X_{(M-1)M}^{(1)}]_{L\times L}[D_{M\pm}^{(1)}]_{L\times 1}. \tag{C1d}$$

Combining Eq. (C1a), with Eqs. (C1b)–(C1d), we have

$$[D_{M\pm}^{(1)}]_{L\times 1}=[X^{(1)}]_{L\times L}^{-1}[X_{11}^{(1)}]_{L\times L}[D_{1\pm}^{(1)}]_{L\times 1}, \tag{C2a}$$

and

$$[X^{(1)}]_{L\times L}=[X_{12}^{(1)}][X_{22}^{(1)}]^{-1}\cdots[X_{(p-1)p}^{(1)}][X_{pp}^{(1)}]^{-1}\cdots[X_{(M-1)\times(M-1)}^{(1)}]^{-1}[X_{(M-1)M}^{(1)}], \tag{C2b}$$

where

$$[D_{p\pm}^{(1)}]_{L\times 1}=[D_{1n+}^{(1,p)}\,D_{2n+}^{(1,p)}\,D_{1n-}^{(1,p)}\,D_{2n-}^{(1,p)}]^T,$$

$$[D_{1\pm}^{(1)}]_{L\times 1}=[D_{1n+}^{(1,1)}\,D_{1n-}^{(1,1)}\,0\;0]^T, \tag{C2c}$$

with the superscript T standing for the transpose of a matrix.

[1] Z. X. Shen, IEE Proc., Part H: Microwaves, Antennas Propag. **141**, 279 (1994).
[2] W. Y. Yin, J. Electromagn. Waves Appl. **10**, 1199 (1996).
[3] W. Y. Yin, H. L. Zhao, and W. Wan, J. Electromagn. Waves Appl. **10**, 1467 (1996).
[4] W. Y. Yin, Micro. Opt. Tech. Lett. **12**, 287 (1996).
[5] J. Jakoby, IEEE Trans. Antennas Propag. **45**, 648 (1997).
[6] K. Konistis and J. L. Tsalamengas, J. Electromagn. Waves Appl. **11**, 1073 (1997).
[7] Dajun Cheng, Y. M. M. Antar, and Gang Wang, Micro. Opt. Tech. Lett. **18**, 410 (1998).
[8] A. Z. Elsherbeni and A. A. Kishk, IEEE Trans. Antennas Propag. **40**, 96 (1992).
[9] M. Ohki, K. Shimizu, and H. Sakurai, Int. J. Electron. **82**, 403 (1997).
[10] V. Dmitriev, Electron. Lett. **34**, 532 (1998).
[11] V. Dmitriev, Electron. Lett. **34**, 743 (1998).
[12] V. Dmitriev, Electron. Lett. **34**, 745 (1998).
[13] V. Dmitriev, Micro. Opt. Tech. Lett. **18**, 280 (1998).
[14] W. S. Weiglhofer and A. Lakhtakia, Micro. Opt. Tech. Lett. **17**, 405 (1998).
[15] W. S. Weiglhofer, A. Lakhtakia, and B. Michel, Micro. Opt. Tech. Lett. **18**, 342 (1998).
[16] W. Y. Yin and I. Wolff, J. Electromagn. Waves Appl. **13**, 259 (1999).